Iranian Journal of Fuzzy Systems

Volume 22, Number 5, (2025), pp. 143-158

Original paper

Dynamic PV modeling using fuzzy logic and genetic algorithm for enhanced monocrystalline array performance

Z. I. Saci[1], M. Bechouat[2], M. Sedraoui[3] and R. Ayaz[4]

[1,2] *Department of Automation and Electromechanics, Faculty of Science and Technology, University of Ghardaia, Ghardaia, Algeria*

[1] *Material, Energy Systems Technology and Environment Laboratory, Faculty of Science and Technology, Université de Ghardaia, BP 455, 47000 Ghardaia, Algeria*

[3] *Laboratory of Inverse Problems, Modeling, Information and Systems (PI:MIS), University 8 Mai 1945 Guelma, Algeria*

[4] *Departmenft of Electrical Engineering, Yildiz Technical University, Davutpasa Campus, 34220 Istanbul, Turkey*

[4] *Clean Energy Technologies Institute, Yildiz Technical University, Davutpasa Campus, 34220 Istanbul, Turkey*

saci.zehourismahane@univ-ghardaia.edu.dz,mohcene@univ-ghardaia.edu.dz, sedraoui.moussa@univ-guelma.dz, ayaz@yildiz.edu.tr

Abstract

This paper proposes a novel photovoltaic (PV) array model using an equivalent single-diode electrical circuit with three time-varying parameters: the diode quality factor, series resistance, and shunt resistance. The goal is to determine an optimal fuzzy inference mechanism to accurately predict the evolution of each parameter under varying climatic conditions, such as solar irradiance, cell temperature, and PV voltage. A dataset of 500 experimental samples, collected from three series-connected monocrystalline PV panels, was used–300 samples for model training and 200 for validation. The proposed design normalizes input data to [0,1] and feeds it into an initial fuzzy mechanism with predefined fuzzification rules. The mechanism generates normalized outputs, which are denormalized to compute predicted PV currents. These are compared to actual measurements to calculate modeling errors, aggregated as mean squared errors (MSEs). A genetic algorithm (GA) minimizes the MSEs by optimizing the fuzzification rules, retaining only the most effective ones. This process iterates until a final fuzzy mechanism with reduced fuzzification rules is achieved, capable of supervising the evolution of each adjustable parameter under varying climatic conditions. Experimental validation confirms the accuracy and robustness of the proposed adjustable-parameter PV model, outperforming conventional fixed-parameter models. This approach provides a reliable framework for PV system modeling, significantly improving predictive accuracy and adaptability in real-world conditions, with potential applications in advanced MPPT controller synthesis and renewable energy system optimization.

Keywords: Photovoltaic modeling, MPPT, fuzzy logic, optimization.

1 Introduction

In renewable energy systems, designing robust Maximum Power Point Tracking (MPPT) controllers is essential to maximize power extraction from solar panels, particularly under unpredictable and rapidly changing climatic conditions or in the presence of partial shading [1, 17, 18]. Accurate modeling of PV arrays is critical for this purpose, as it minimizes the gap between predicted and actual performance. Traditional PV models with fixed parameters are based on equivalent electrical circuits, incorporating diodes, series resistances, and shunt resistances, with current outputs heavily dependent on solar irradiance, outdoor temperature, and wind speed [4]. These models rely on three key parameters, typically identified through analytical or numerical methods. While analytical approaches provide precise solutions, they involve solving complex, nonlinear equations, making them challenging to implement [4, 30]. As a

Corresponding Author: M. Bechouat

Received: April 2025; Revised: July 2025; Accepted: September 2025.

https://doi.org/10.22111/ijfs.2025.51625.9126

result, researchers often turn to numerical methods, employing heuristic and metaheuristic optimization algorithms to identify these parameters by minimizing a fitness function that compares predicted and measured current outputs. For instance, El-Naggar et al. (2012) used simulated annealing (SA) to identify parameters in single- and double-diode models [14], while Ismail et al. (2013) applied GA for global optimization [19]. Askarzadeh and Leandro dos Santos (2015) introduced the simplified bird mating optimizer (SBMO) [6], and Alam et al. (2015) utilized the flower pollination (FP) algorithm [3]. Bechouat et al. (2017) compared the performances of both particle swarm optimization (PSO) and GA for parameter identification in fixed-parameter PV models[10]. More recently, Yang et al. (2020) provided a comprehensive review of metaheuristic algorithms for PV parameter identification [29], and Diab et al. (2020) proposed the coyote optimization algorithm (COA) for estimating parameters in various solar cell models [13]. Wang et al. (2021) enhanced parameter estimation using an improved equilibrium optimizer algorithm [27], while Premkumar et al. (2021) introduced a gradient-based optimization algorithm with chaotic drifts [24]. Bo et al. (2022) developed a robust niching chimp optimization algorithm [11], and Al-Subhi et al. (2024) leveraged optimized deep neural networks for PV parameter estimation [5]. Izci et al. (2024) proposed an enhanced prairie dog optimization algorithm[20], and Tang et al. (2025) introduced a parameter-adaptive manta ray foraging optimization algorithm [26]. Çelik et al. (2025) further advanced the field by reconfiguring single- and double-diode models for improved accuracy [12]. Despite these advancements, fixed-parameter PV models face significant limitations. They assume constant values for key parameters, failing to capture the dynamic behavior of PV arrays under varying climatic conditions. This leads to substantial modeling errors, particularly during sudden environmental changes, and limits their adaptability in real-world scenarios. Optimization algorithms used for fixed-parameter models often converge to local optima, resulting in inaccurate parameter identification and reduced reliability. Additionally, these models heavily depend on specific experimental datasets, which may not represent all operating conditions, further limiting their generalization and robustness. To address these challenges, researchers have proposed dynamic PV models with time-varying parameters. For example, Górecki and Krac (2016) focused on measuring thermal parameters of solar modules to improve dynamic modeling accuracy [16]. Gontean et al. (2017) introduced a high-accuracy PV cell model incorporating self-heating and parameter variations, significantly enhancing modeling precision [15]. Kazemian et al. (2021) and Wen et al. (2022) explored advanced photovoltaic thermal systems integrated with phase change materials (PCM) and thermoelectric generators (TEG), further optimizing performance under varying conditions [22, 28]. Kahla et al. (2022) proposed a dynamic PV model where series and shunt resistors were replaced with metallic or thermistor elements, enabling parameter variations fitted by nonlinear functions dependent on outdoor temperature [21]. Lappalainen et al. (2024) highlighted the challenges of identifying series resistance in PV modules under maximum power production, emphasizing the computational burden of nonlinear models [23]. While these dynamic models offer improved accuracy and adaptability, they also introduce notable drawbacks. The inclusion of nonlinear thermal parameters increases the search space and degree-of-freedom of the optimization problem, making controller synthesis more complex and computationally intensive. This complexity limits their practicality for real-time applications and increases the risk of convergence issues in optimization algorithms. Given these challenges, this paper proposes a novel PV model with adjustable parameters that avoids nonlinear complexities. The evolution of these parameters is supervised by a fuzzy logic mechanism, where its fuzzification rules are optimally determined using the GA. Unlike fixed-parameter models, this approach dynamically adapts to changing conditions, significantly improving modeling accuracy and adaptability. The proposed PV model is validated using experimental data, demonstrating its superior performance in terms of modeling error and robustness compared to traditional fixed-parameter models. The paper is structured as follows: Section 2 details the modeling of the standard PV model with three fixed parameters, including parameter determination using the Lambert W function and constrained optimization. Section 3 introduces the proposed adjustable-parameters PV model, where parameter evolution is supervised by a fuzzy mechanism with GA-optimized fuzzification rules. Section 4 presents experimental validation, comparing the performance of the standard and proposed PV models. The paper concludes with suggestions for future research in PV array modeling with adjustable parameters using advanced supervisory techniques.

2 Design of the standard fixed-parameter PV model

2.1 Equivalent electrical circuit for a PV array

In general, connecting N_s PV panels in series forms a single PV string, where each PV panel consists of N_c PV cells connected in series. Additionally, connecting N_p PV strings in parallel forms a single PV array. The primary objective of this section is to model this PV array using a fixed-parameter PV model. Typically, the PV model is based on a nonlinear equation that relates the predicted global PV current I_m^g to the global PV voltage V_m^g. This equation is derived from an equivalent electrical circuit, which includes the following components:

- A fixed global series resistance R_s^g, where $R_s^g = \left(\frac{N_s}{N_p}\right) \cdot R_s^1$.
  Here, R_s^1 represents the internal and contact resistances of a PV cell.
- A fixed global shunt resistance R_p^g, where $R_p^g = \left(\frac{N_s}{N_p}\right) \cdot R_p^1$.
  Here, R_p^1 represents the leakage currents within a PV cell.
- A fixed diode quality factor n.

The relationship between I_m^g and V_m^g is illustrated in Figure 1 and expressed by Equation 1[21]:

$$I_m^g = I_{ph}^g - I_{od}^g \cdot \left(-1 + \exp\left(\frac{V_m^g + R_s^g \cdot I_m^g}{n \cdot V_T^g}\right)\right) - \left(\frac{V_m^g + R_s^g \cdot I_m^g}{R_p^g}\right). \tag{1}$$

Where V_T^g is the global thermal voltage of the PV array, given by $V_T^g = N_s \cdot V_T^1$. The thermal voltage of a single diode V_T^1 is generated by N_c number of series-connected PV cells within a single PV panel. It is expressed as [2, 9]:

$$V_T^1 = \left(\frac{k \cdot T_c}{q}\right) \cdot N_c. \tag{2}$$

Where $q = 1.602176 \times 10^{-19}$ C is the electronic charge, and $k = 1.3806503 \times 10^{-23}$ J/K is the Boltzmann constant.

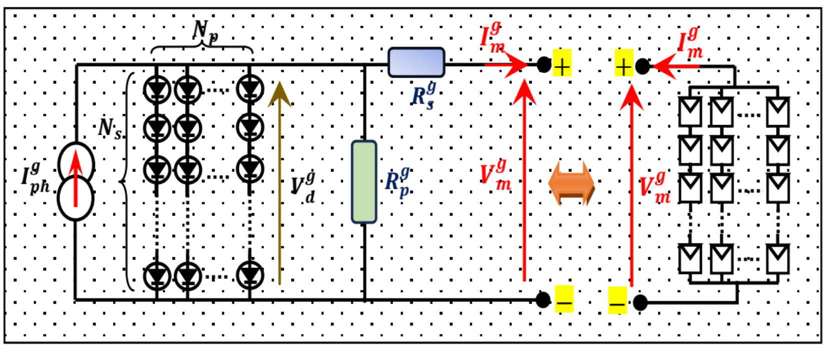

Figure 1: Equivalent electrical-circuit used for modelling the PV array

Cell temperature T_c is determined as a function of outdoor temperature T, solar irradiance G, and wind speed ω using the empirical relationship [8]:

$$T_c = 1.14 \cdot (T - T_{\text{stc}}) + 0.0175 \cdot (G - 300) - K_r \cdot \omega + 30. \tag{3}$$

Where K_r is a positive parameter provided in the manufacturer's data sheet.
The global photo-current I_{ph}^g is given by $I_{ph}^g = N_p \cdot I_{ph}^1$, where I_{ph}^1 is the photo-current corresponding to a single PV panel. It is defined by [7]:

$$I_{ph}^1 = \left(\frac{G}{G_{\text{stc}}}\right) \cdot \left(I_{\text{sh},0}^1 + \alpha \cdot (T_c - T_{\text{stc}})\right). \tag{4}$$

Where $T_{\text{stc}} = 25\,C$ and $G_{\text{stc}} = 1000\,\text{W} \cdot \text{m}^{-2}$ are the nominal outdoor temperature and nominal solar irradiance under Standard Test Conditions (STC), respectively. The parameter α is the temperature coefficient of the nominal short-circuit current $I_{\text{sh},0}^1$ for a single PV panel.

Moreover, the global reverse saturation current I_{od}^g is defined by $I_{od}^g = N_p \cdot I_{od}^1$, where I_{od}^1 is the reverse saturation current of the diode corresponding to a single diode. It can be derived from the datasheet information as [7]:

$$I_{od}^1 = I_{\text{sr}}^1 \cdot \left(\frac{T_c}{T_{\text{stc}}}\right)^{3/n} \cdot \exp\left(\frac{q \cdot E_g}{k \cdot n} \cdot \left(\frac{1}{T_{\text{stc}}} - \frac{1}{T_c}\right)\right), \tag{5}$$

where E_g is the band-gap energy of the semiconductor across the diode and I_{sr}^1 is the diode current for a single diode. It is given by [7]

$$I_{sr}^1 = \frac{I_{sh,0}^1 + \alpha \cdot (T_c - T_{stc})}{-1 + \exp\left(\frac{V_{oc}^1 + \beta \cdot (T_c - T_{stc})}{n \cdot V_T^1}\right)}, \tag{6}$$

where V_{oc}^1 is the open-circuit voltage for a single PV panel, and β is the temperature coefficient corresponding the monocrystalline technology of the PV panel.

2.2 Analytical solution based on LambertW for predicted global current computation

The primary objective of this work is to enhance the accuracy of the global PV model to faithfully replicate the actual behavior of the PV array. This accuracy hinges not only on the proper optimization of the three key parameters mentioned earlier but also on determining the exact root of the nonlinear function (f), derived from Equation 1 and expressed as:

$$f(I_m^g) = I_m^g - I_{ph}^g + I_{od}^g \cdot \left(-1 + \exp\left(\frac{V_m^g + R_s^g \cdot I_m^g}{n \cdot V_T^g}\right)\right) + \left(\frac{V_m^g + R_s^g \cdot I_m^g}{R_p^g}\right). \tag{7}$$

The resulting root represents the best predicted global PV current vector I_m^g. Its computation requires substituting the vector V_m^g with the actual global PV voltage V_{pv}^g and reformulating Equation 1 in the general form:

$$Z = W(X).e^{W(X)}. \tag{8}$$

Z is the argument of the real function $W(X)$, and $e^{W(X)}$ includes the real vector X. This vector presents the solution of Equation 7, expressed in the general form:

$$X = lambertW(Z). \tag{9}$$

From mathematical developments of Equation 1 in accordance with the general form above, we can obtain [8, 22].

$$X = \left(\frac{R_s^g.R_p^g}{n.V_T^g.(R_p^g + R_s^g)}\right).I_{od}^g.\exp\left(\frac{V_m^g + R_s^g.I_m^g}{n.V_T^g}\right). \tag{10}$$

$$Z = \left(\frac{R_s^g.R_p^g}{n.V_T^g.(R_p^g + R_s^g)}\right).I_{od}^g.\exp\left(\frac{R_s^g.R_p^g}{n.V_T^g(R_p^g + R_s^g)}\left(I_{ph}^g + I_{od}^g + \frac{V_m^g}{R_s^g}\right)\right). \tag{11}$$

The predicted global PV current $\hat{I}_m^g$ is finally expressed as [21, 25]

$$\hat{I}_m^g = \frac{R_p^g \cdot (I_{ph}^g + I_{od}^g) - V_m^g}{R_p^g + R_s^g} - \frac{n \cdot V_T^g}{R_s^g} \cdot \text{LambertW}(Z). \tag{12}$$

2.3 Constrained optimization problem for identifying fixed parameters of the conventional PV model

Once the analytical determination of the predicted global current $\hat{I}_m^g$ is completed, it is necessary to compare it with the corresponding measured current vector I_{pv}^g at each sample point (k). This comparison allows the definition of a fitness function to be minimized, such as the Mean Squared Error (MSE), Integral Time Absolute Error (ITAE), or similar criterion. Since the choice of criterion does not significantly impact the optimization results and is not part of the contribution of this paper, the MSE criterion is adopted as the fitness to be minimize. Furthermore, while numerous heuristic and metaheuristic algorithms are capable of solving this modeling problem effectively, the GA among is chosen as the optimizer for this study. This choice is also not part of the paper's contribution but is made for its effectiveness in handling such optimization tasks. The PV model design with fixed parameters can be formulated as the following constrained optimization problem [25]:

$$\min_{\substack{n_{\min} \le n \le n_{\max} \\ R_{s\,\min}^g \le R_s^g \le R_{s\,\max}^g \\ R_{p\,\min}^g \le R_p^g \le R_{p\,\max}^g}} J = \frac{1}{N} \cdot \sum_{k=1}^{N} \left(\hat{I}_m^g(k, n, R_s^g, R_p^g) - I_{pv}^g(k)\right)^2, \tag{13}$$

where N is the number of total samples collected during the experimental test. Finally, the optimal resulting three fixed parameters n^*, R_s^{g*}, and R_p^{g*} also lead to determine the global diode voltage V_d^g where $V_d^g = V_m^g + R_s^{g*} \cdot I_m^g$ (see Figure 1).

3 Design of the proposed adjustable-parameters PV model

The proposed methodology is illustrated in Figure 2. Initially, real-time input data measurements are normalized and fuzzified using predefined membership functions. A primary fuzzy inference system, equipped with user-defined fuzzification rules, computes three normalized parameters of the global PV model through defuzzification step using corresponding membership functions. These outputs are denormalized and, combined with the input dataset, used to compute the initial predicted global PV current using Equation 12. The MSE criterion is calculated by comparing the predicted global PV current, resulting from each fuzzification rule, with the actual global measured PV current. The GA minimizes the total MSEs, updating the initial fuzzification rules accordingly. The updated fuzzification rules are reorganized in descending order of their MSE contributions, retaining only those with the lowest MSE values for the next GA generation. This iterative process continues until the final optimal fuzzy mechanism is achieved.

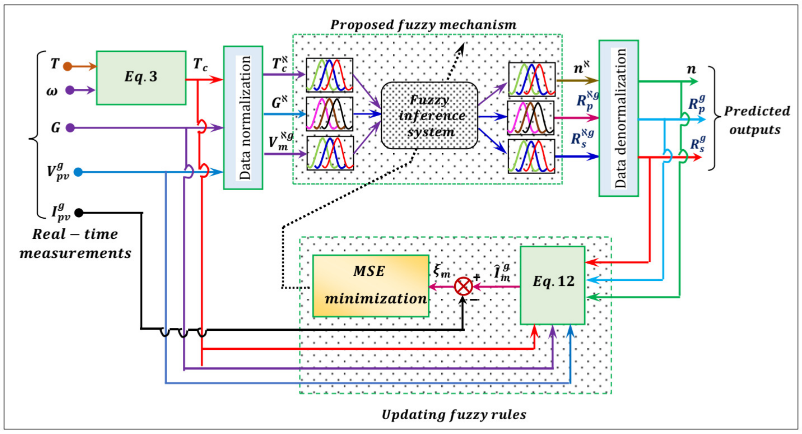

Figure 2: Three adjustable extraction parameters for global PV model using the proposed fuzzy mechanism

This last one will be used to supervise the evolution of each adjustable parameter of the proposed global PV model under varying climatic conditions. A key aspect of this approach is the GA-based updating of fuzzification rules in the inference system, ensuring continuous refinement and optimization of the model.

3.1 GA-based updating of fuzzification rules in the proposed fuzzy mechanism

a) ***Fuzzy model structure***

The fuzzy model takes the normalized input vector $X^{\aleph} = (G^{\aleph}, T_c^{\aleph}, V_m^{\aleph_g})^T$, derived from the real measurement vector $X = (G, T_c, V_m^g)^T$ and its lower and upper bound vectors X_{min} and X_{max} using Equation 14:

$$X^{\aleph} = f^{\aleph}(X) = \frac{X - \min(X)}{\max(X) - \min(X)}. \tag{14}$$

Here, $G^{\aleph}$,$T_c^{\aleph}$ and $V_m^{\aleph_g}$ are the normalized solar irradiance, normalized cell temperature and normalized global PV voltage respectively. The proposed fuzzy model predicts the normalized output vector $Y^{\aleph} = (n^{\aleph}, R_s^{\aleph_g}, R_P^{\aleph_g})^T$, where:

- $n^{\aleph}$ is the normalized predicted diode quality factor,
- $R_s^{\aleph_g}$ is the normalized predicted global series resistance,
- $R_p^{\aleph_g}$ is the normalized global shunt resistance.

The denormalized vector $Y^{\mathfrak{D}}$ is derived from $Y^{\aleph}$ and its lower and upper bound vectors $\min(Y)$ and $\max(Y)$, computed by Equation 15:

$$Y^{\mathfrak{D}} = f^{\mathfrak{D}}(Y^{\aleph}) = \min(Y) + Y^{\aleph} \cdot (\max(Y) - \min(Y)). \tag{15}$$

The lower bound $\min(Y)$ vector has the user-preselected constants $n^{\aleph}_{min}$, $R^{\aleph_g}_{s_{min}}$ and $R^{\aleph_g}_{p_{min}}$, while the upper bound vector $\max(Y)$ includes the user-preselected constants $n^{\aleph}_{max}$, $R^{\aleph_g}_{s_{max}}$ and $R^{\aleph_g}_{p_{max}}$.

b) *Fuzzification of normalized inputs*

Each component of the normalized input vector $X^{\aleph}$ is fuzzified using five membership functions, corresponding to the linguistic states: **Big Small (BS,1)**, **Small (S,2)**, **Medium (M,3)**, **High (H,4)**, and **Big High (BH,5)**. The membership functions for the normalized inputs $G^{\aleph}$,$T_c^{\aleph}$ and $V_m^{\aleph g}$ are denoted $\mu_{G^{\aleph}}$,$\mu_{T_c^{\aleph}}$ and $\mu_{V_m^{\aleph g}}$ respectively.

c) *Fuzzy inference system*

The fuzzy inference system contains a set of fuzzification rules, each rule R_i is initially set by the user. The general form of the i^{th} fuzzification rule and j^{th} linguistic state is:

$$\begin{aligned} R_i : \textbf{If } G^{\aleph} \textbf{ is } \left\{\mu_{G^{\aleph}}^{(i,j)}\right\} \textbf{ and } T_c^{\aleph} \textbf{ is } \left\{\mu_{T_c^{\aleph}}^{(i,j)}\right\} \textbf{ and } V_m^{\aleph g} \textbf{ is } \left\{\mu_{V_m^{\aleph g}}^{(i,j)}\right\}, \\ \textbf{then } n^{\aleph} \text{ is } \left\{\mu_{n^{\aleph g}}^{(i,j)}\right\} \textbf{ and } R_p^{g\aleph} \textbf{ is } \left\{\mu_{R_p^{g\aleph}}^{(i,j)}\right\} \text{ and } R_s^{g\aleph} \textbf{ is } \left\{\mu_{R_s^{g\aleph}}^{(i,j)}\right\} \end{aligned} \tag{16}$$

Here:

- $\mu_{G^{\aleph}}^{(i,j)}$, $\mu_{T_c^{\aleph}}^{(i,j)}$ and $\mu_{V_m^{\aleph g}}^{(i,j)}$ are the degrees of membership of the inputs $G^{\aleph}$, $T_c^{\aleph}$ and $V_m^{\aleph g}$, respectively, for the i^{th} fuzzification rule and j^{th} linguistic state,
- $\mu_{n^{\aleph g}}^{(i,j)}$, $\mu_{R_p^{g\aleph}}^{(i,j)}$ and $\mu_{R_s^{g\aleph}}^{(i,j)}$ are the degrees of membership of the outputs $n^{\aleph}$, $R_p^{g\aleph}$ and $R_s^{g\aleph}$, respectively, for the i^{th} fuzzification rule and j^{th} linguistic state.

  where $j = 1, 2, 3, 4, 5$ is the linguistic state index and $i = 1, \dots, 125$ is the fuzzification rule index.

d) *Defuzzification of outputs*

The defuzzied outputs are computed using the **center of gravity method**:

$$n^{\aleph} = \frac{\sum_{i=1}^{r}\left(\sum_{j=1}^{5}\left(\mu_{G^{\aleph}}^{(i,j)} \cdot \mu_{T_C^{\aleph}}^{(i,j)} \cdot \mu_{V_m^{\aleph g}}^{(i,j)} \cdot \mu_{n^{\aleph g}}^{(i,j)} \cdot n_i^{\aleph}\right)\right)}{\sum_{i=1}^{r}\left(\sum_{j=1}^{5}\left(\mu_{G^{\aleph}}^{(i,j)} \cdot \mu_{T_C^{\aleph}}^{(i,j)} \cdot \mu_{V_m^{\aleph g}}^{(i,j)}\right)\right)}. \tag{17}$$

$$R_p^{g\aleph} = \frac{\sum_{i=1}^{r}\left(\sum_{j=1}^{5}\left(\mu_{G^{\aleph}}^{(i,j)} \cdot \mu_{T_C^{\aleph}}^{(i,j)} \cdot \mu_{V_m^{\aleph g}}^{(i,j)} \cdot \mu_{R_p^{g\aleph}}^{(i,j)} \cdot R_{p,i}^{g\aleph}\right)\right)}{\sum_{i=1}^{r}\left(\sum_{j=1}^{5}\left(\mu_{G^{\aleph}}^{(i,j)} \cdot \mu_{T_C^{\aleph}}^{(i,j)} \cdot \mu_{V_m^{\aleph g}}^{(i,j)}\right)\right)}. \tag{18}$$

$$R_s^{g\aleph} = \frac{\sum_{i=1}^{r}\left(\sum_{j=1}^{5}\left(\mu_{G^{\aleph}}^{(i,j)} \cdot \mu_{T_C^{\aleph}}^{(i,j)} \cdot \mu_{V_m^{\aleph g}}^{(i,j)} \cdot \mu_{R_s^{g\aleph}}^{(i,j)} \cdot R_{s,i}^{g\aleph}\right)\right)}{\sum_{i=1}^{r}\left(\sum_{j=1}^{5}\left(\mu_{G^{\aleph}}^{(i,j)} \cdot \mu_{T_C^{\aleph}}^{(i,j)} \cdot \mu_{V_m^{\aleph g}}^{(i,j)}\right)\right)}. \tag{19}$$

Here:

- $n_i^{\aleph}$, $R_{p,i}^{g\aleph}$ and $R_{s,i}^{g\aleph}$ are the normalized output values of $n^{\aleph}$, $R_p^{g\aleph}$ and $R_s^{g\aleph}$ for the i^{th} fuzzification rule,
- r is the total number of the fuzzification rules, $r = 125$.

e) *GA for fuzzification rule optimization*

The GA is used to optimize the fuzzification rules from minimizing the MSE criterion corresponding each fuzzification rule R_i where each MSE is generated from comparing the predicted output $I_{m,i}^g$ and the real measured output I_{pv}^g. Here, $I_{m,i}^g$ is computed using the denormalized outputs n, R_p^g and R_s^g of each fuzzification rule R_i and the real inputs G, T_c and V_m^g using Equation 12.

f) *Encoding and Optimization of Fuzzy Rules*

Each fuzzy rule R_i is encoded as a chromosome in the GA. The chromosome for the i^{th} fuzzification rule given by: $[G_i^{\aleph}, T_{c_i}^{\aleph}, V_{m_i}^{\aleph g}, n_i^{\aleph}, R_{p,i}^{g\aleph}, R_{s,i}^{g\aleph}]$, where the first three components $G_i^{\aleph}$,$T_{c_i}^{\aleph}$ and $V_{m_i}^{\aleph g}$ are fixed combinations ($e.g.$, 111, 112, ..., 555), while the last three components $n_i^{\aleph}$,$R_{p,i}^{g\aleph}$ and $R_{s,i}^{g\aleph}$ are optimized by the GA. This algorithm searches for the optimal combination of output states among all possible combinations ($e.g.$, $(BS)(BS)(BS)$, $(BS)(BS)(BS), \dots, (BH)(BH)(BH)$. This involves optimizing three integer variables within the lower bound vector $L_B = [1\ 1\ 1]^T$, and the upper bound $U_B = [5\ 5\ 5]^T$.

g) *Reduction of Fuzzy Rules*

To reduce the number of fuzzification rules, the GA evaluates the MSE contribution of each rule. The rules are ranked in descending order of their MSE contributions, and only the top rules are retained for the next generation. This ensures that the final fuzzy model has a reduced number of rules while maintaining high accuracy.

3.2 Formulation of the optimization problem

The optimization problem can be formulated as:

$$\begin{array}{l} \text{Minimize } J = \frac{1}{N} \cdot \sum_{k=1}^{N} \left\{ \hat{I}_{m}^{g}(k) - I_{pv}^{g}(k) \right\}^2, \\ \text{Subject to: } \left\{ \mu_{n^{\aleph}}^{(j)}, \mu_{R_p^{g\aleph}}^{(j)}, \mu_{R_s^{g\aleph}}^{(j)} \right\} \in \{1, 2, 3, 4, 5\}. \end{array} \tag{20}$$

4 Performance assessments for standard and proposed PV models

4.1 Experimental test description

The experimental test was conducted using a set of PV panels installed on the roof of the faculty at Yildiz University, Istanbul, Turkey [7, 25]. The PV panels included three types: thin-film, monocrystalline, and polycrystalline. This study focuses on monocrystalline panels, as the other types yielded similar results. The PV array consisted of three panels connected in series to achieve the desired current and voltage levels. Initially, modeling was performed using an equivalent electrical circuit with fixed parameters optimized by the GA algorithm. Subsequently, an equivalent electrical circuit with adjustable parameters was employed, where parameters were supervised by the proposed fuzzy mechanism based on fuzzification rule updating using the GA. The modeling phase utilized a subset of 300 samples, while the validation phase used a separate subset of 200 samples. Data were collected hourly over a one-month period, starting at 9 a.m. on September 9th, 2024, resulting in 500 samples of total current I_{pv}^{g} and voltage V_{pv}^{g}, solar irradiance G (measured using a Kipp-Zonen CMP21 pyranometer), outdoor temperature T (measured using a Campbell CS215 thermocouple), and wind speed ω (measured using a tachymeter). Figure 3 illustrates the experimental setup, including the various measuring instruments [7, 25].

Figure 3: PV panels and measuring equipment used in the experimental test

The minimum and maximum values recorded for each measurement during the one-month period are summarized in Table 1 given below.

Table 1: Minimum and maximum limits recorded for all real-time measurements during one month

	I_{PV}^{g} (A)	V_{PV}^{g} (V)	G (W· m^{-2})	T (°C)	ω (m· s^{-1})
minimum value	0	1.0042	0	13.600	0.2133
maximum value	8.2634	102.25	759.47	32.712	26.658

From the upper and lower limits summarized in Table 1, it is evident that STC conditions were not achieved during the specified period. Since the performance assessment of any control strategy must be conducted under STC, the goal is to design an efficient equivalent electrical circuit that can ensure accurate predictions not only under STC conditions but also for any random variations in the aforementioned conditions.

4.2 Computation of the fixed parameters of the standard PV model

The datasheet for a single PV panel based on monocrystalline technology is summarized in Table 2 below

Table 2: Data sheet monocrystalline one PV panel based on polycrystalline technology

Parameter		Value	Unit
	P_{stc}^{1}	915.564	W
	V_{stc}^{1}	99.33	V
	$V_{oc,stc}^{1}$	119.82	V
	I_{stc}^{1}	9.22	A
	$I_{sc,stc}^{1}$	9.71	A
α		0.04	$\%$ / $°C$
β		-0.32	$\%$ / $°C$
K_r		1.509	–

The primary objective is to design a model that accurately describes the behavior of the PV array utilizing the monocrystalline technology. Due to the stochastic nature of the GA algorithm, it is run multiple times to optimally determine the three key fixed parameters of the equivalent electrical circuit. The first dataset, comprising 300 samples, was used for parameter identification. The GA tuning parameters are summarized in Table 3 below.

Table 3: GA setting parameters to solve the design model problem of the overall PV array

Parameters	Value
Population size	20
Plot function	*@gaplotbestf*
Max. nbr. of generations	50
Mutation function	*@mutationadaptfeasible*
Crossover function	*@selectiontournament*
Selection function	$[0.1, 1.1]$
Number of elite counts	2
Crossover Fraction	0.8
Stall generation limit	20
Function tolerance	$10^{-}6$

The search space for the constrained optimization problem was selected after several GA runs. Extensions were performed when the solution became stuck in saturated constraints. The most appropriate choice to avoid saturation is as follows:

$$\begin{aligned} 0.56 &\leq n \leq 1.45, \\ 0.1 &\leq R_s^g \leq 1.5, \\ 1500 &\leq R_p^g \leq 2500. \end{aligned} \tag{21}$$

4.3 Computation of adjustable parameters for the proposed PV model

In this design, the proposed fuzzy mechanism consists of three normalized inputs, three normalized outputs, and five membership functions for each input and output. The sigmoid function was chosen in each membership function for the following linguistic states: (BS), (S), (M), (H), and (BH). For the fuzzification rules, the three normalized inputs are kept by all possible fixed combinations ($e.g.$, $111, 112, ..., 555$), while the three normalized outputs are kept by $(111, 112, ..., 555)$. The GA tuning parameters are conserved as those mentioned in Table 3, and only the top 10 fuzzification rules corresponding the lowest MSE values are retained for the next generation are given in Table 4.

Table 4: The best updates for Rules using GA

Rule #	Irradiance	Temperature	Voltage	R_s	R_p	n
1	*BS*	*BS*	*BS*	*S*	*S*	*S*
2	*S*	*BS*	*BS*	*S*	*S*	*S*
3	*M*	*BS*	*BS*	*S*	*S*	*M*
4	*H*	*BS*	*BS*	*BS*	*M*	*S*
5	*BH*	*BS*	*BS*	*M*	*M*	*BS*
6	*BS*	*S*	*BS*	*BS*	*S*	*S*
7	*S*	*S*	*BS*	*S*	*S*	*S*
8	*M*	*S*	*BS*	*S*	*M*	*M*
9	*H*	*S*	*BS*	*M*	*S*	*S*
10	*BH*	*BS*	*S*	*S*	*M*	*BS*

The minimization process based on GA consistently achieves significant reductions in MSE across numerous runs. The best result yields the lowest MSE value of **0.025** (see Figure 4), representing a substantial improvement compared to the MSE obtained by the fixed-parameter PV model. This corresponds to an improvement rate of approximately **93.77%**, highlighting the effectiveness and value of the proposed approach.

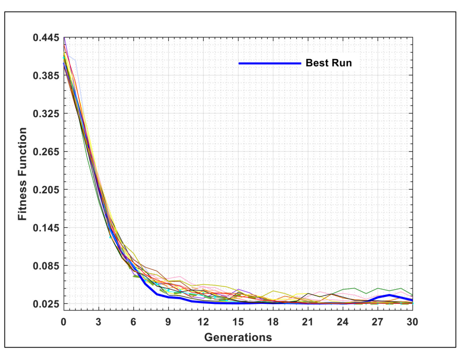

Figure 4: Best MSE minimization using the GA algorithm

4.4 Validation of the optimal GA solution

The optimal solution obtained by the GA algorithm provides the best prediction of the global PV current, which is compared with the actual current for the 300 samples. Figure 5 illustrates the comparison between predicted and actual global PV currents, also depicts the corresponding modeling accuracy achieved during the parameter identification process for the PV model with adjustable parameters.

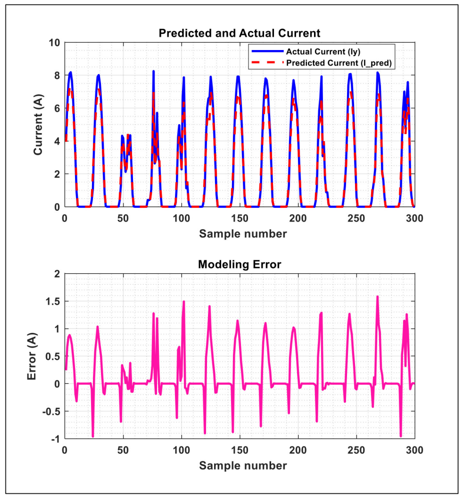

Figure 5: Actual and predicted global PV currents and modeling error provided during Fuzzy Model Design

Figure 6 illustrates the evolution of each model parameter during the validation phase. The results reveal significant fluctuations in the model parameters, demonstrating that the actual behavior of the PV array cannot be effectively captured by a model with fixed parameters.

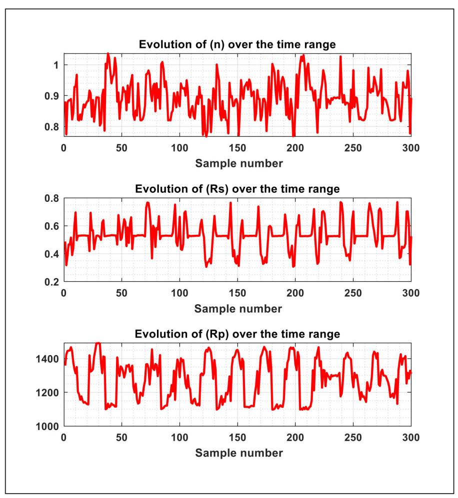

Figure 6: Evolution of three adjustable parameters during Fuzzy Model Design

Figure 7 illustrates the membership functions Gaussian shapes of the optimum fuzzy system designed. The membership functions represent the fuzzy sets for the input or output variables of the system, used by the GA to achieve the best performance for a specific application. Each membership function is typically plotted as a curve on a graph, where the $x - axis$ represents the range of the input or output variable, and the $y - axis$ represents the degree of membership, ranging from 0 to 1.

Figure 8 presents a 3D surface plot illustrating the nonlinear input-output mapping of the proposed fuzzy logic system, where the x- and y-axes represent normalized solar irradiance ($G^{\aleph}$) and cell temperature ($T_c^{\aleph}$), while the z-axis denotes the predicted normalized global series resistance ($R_s^{\aleph g}$), the predicted normalized shunt resistance $R_p^{\aleph g}$ and the predicted normalized diode ideal factor $n^{\aleph}$. For the case of the normalized global series resistance $R_s^{\aleph g}$, the surface exhibits a piecewise-continuous topology with distinct gradients, reflecting the system's adaptive response to dynamic climatic conditions. For instance, at low irradiance ($G^{\aleph} = 0.2$) and temperature ($T_c^{\aleph} = 0.3$), the series resistance $R_s^{\aleph g}$ converges to $\sim$0.15 (normalized), while at high irradiance ($G^{\aleph} = 0.8$) and temperature ($T_c^{\aleph} = 0.7$), it peaks at $\sim$0.45, demonstrating a 200% increase. This variability underscores the inadequacy of fixed-parameter models, which assume a constant $R_s^{\aleph g}$ (e.g., 0.82 Ω as per GA-optimized baseline). Sharp transitions near ($G^{\aleph} = 0.5$, $T_c^{\aleph} = 0.5$) indicate rule activation thresholds, validated by the 93.77% MSE reduction achieved through GA-optimized fuzzy rules. The surface's

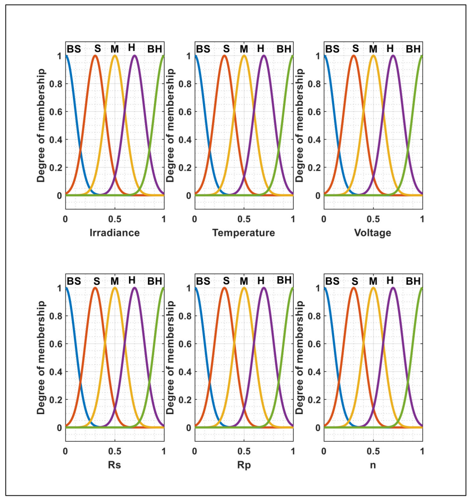

Figure 7: Membership functions of the fuzzy system: Gaussian Shapes

smooth interpolation between linguistic states (BS to BH) confirms the system's robustness in handling stochastic environmental fluctuations, aligning with experimental validation results where parameter adaptability reduced modeling errors to **0.025** MSE compared to **0.41** MSE for fixed-parameter models.

Figure 8 depicts the nonlinear relationship between two normalized input variables (e.g., solar irradiance $G^{\aleph}$ and cell temperature $T_c^{\aleph}$) and one denormalized output parameter (e.g., series resistance $R_s^{\aleph g}$) of the fuzzy logic system, showcasing piecewise-continuous slopes with peaks and valleys that reflect rule-dominated regions (e.g., high irradiance/low temperature) and smooth transitions between linguistic states. The surface's sharp edges indicate boundaries where membership functions overlap minimally, while flat regions reveal insensitivity to certain input variations, aligning with PV saturation effects. The absence of erratic oscillations confirms the GA-optimized rule set's robustness (Table 6), avoiding overfitting and generalizing well to unseen data, as validated by the low MSE in Table 5. This visualization underscores the fuzzy mechanism's ability to dynamically adapt PV parameters to climatic changes, bridging empirical data with theoretical models while maintaining interpretability and accuracy.

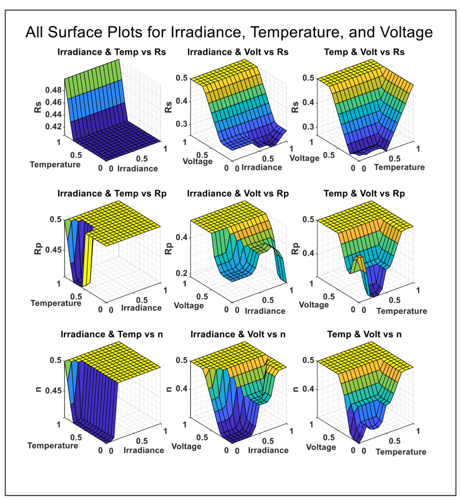

Figure 8: 3D surface plot of fuzzy logic system input-output mapping

4.5 Validation of the fuzzy PV model

The Fuzzy model is reconstructed using the optimal rules derived from the GA algorithm. To evaluate its accuracy and generalization capability, the model is tested on a second dataset comprising 200 additional samples. During this validation phase, the performance of the PV model with adjustable parameters is assessed to ensure its ability to accurately predict the behavior of the PV array under varying conditions. Figure 9 illustrates the evolution of each model parameter during the validation phase. The results reveal significant fluctuations in the model parameters, demonstrating that the actual behavior of the PV array cannot be effectively captured by a model with fixed parameters. In contrast, the proposed PV model, supervised by the Fuzzy with GA-based updates, provides a more accurate representation of the PV array's performance. This is clearly demonstrated in Figure 10, where the predicted global PV current closely aligns the actual measurements, even for new data points not included in the parameter identification step. Also, it presents a comparison of the modeling errors between the two PV models: one with fixed parameters and the other with adjustable parameters. The results clearly demonstrate that the proposed PV model with adjustable parameters achieves the lowest error, confirming its superiority in addressing this type of modeling problem.

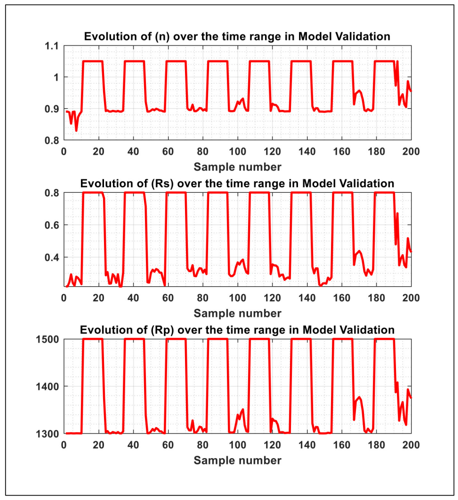

Figure 9: Evolution of three adjustable parameters during Fuzzy model validation

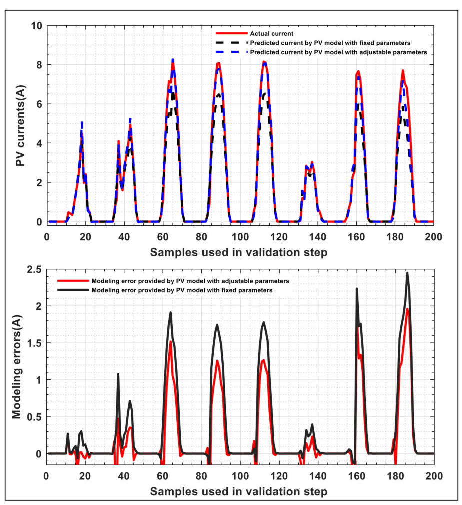

Figure 10: Comparison of Predicted Global PV Currents and Modeling Errors during Fuzzy Model Validation

4.6 Performance robustness and design justifications

The performance achieved by the proposed three-adjustable-parameter PV model demonstrates a significant leap and remarkable gain in modeling not only monocrystalline solar panels but also polycrystalline and thin-film technologies. The real-time evolution of these three parameters relies on the proposed fuzzy mechanism, whose design raises several critical questions:

4.6.1 Training sample size robustness

- *Is the choice of 300 input-output measurement points sufficient to confirm the success of the parameter identification stage?*
- *Does selecting 200 input-output measurements ensure validity under all possible unpredictable climatic conditions?*

To address these concerns, an empirical analysis was performed by varying the number of training samples (from 50 to 300) while reserving 200 samples for validation. The results (Table 5) demonstrate that the model's MSE stabilizes after 200–250 samples, with marginal improvements beyond this point.

Table 5: Model performance across varying training sample sizes

Training Samples	Training MSE	Validation MSE
50	0.042	0.045
100	0.035	0.038
150	0.029	0.032
200	0.026	0.028
250	0.025	0.027
300	**0.025**	**0.026**

According to Table 5, it is easy to confirm the following key findings, summarized as below:

- Training MSE plateaus at **0.025** with 250+ samples (**93.77%** improvement over smaller datasets).
- Validation MSE closely tracks training error (**0.026–0.028**), confirming generalization capability.

As a result, the model achieves robust performance with **200–250** samples, making it practical for real-world deployment without excessive data requirements.

4.6.2 Optimality of fuzzy rule count

- Is the choice of **125 fuzzy rules** (5 membership functions per input) truly optimal?
- Could a higher or lower number of membership functions improve efficiency?

We evaluated rule counts from **27** (3 MF/input) to **343** (7 MF/input). The results are summarized in Table 6.

Table 6: Rule Count vs. Performance

Number of Rules	Training MSE	Validation MSE
27 (3 MF/input)	0.041	0.044
64 (4 MF/input)	0.033	0.036
125 (5 MF/input)	**0.025**	**0.026**
216 (6 MF/input)	0.024	0.025
343 (7 MF/input)	0.023	0.024

According to Table Table 6, it is easy to show the following key finding:

- **125 rules (5 MF/input)** strike the optimal balance:
  - Lowest MSE (0.025) with reasonable computational cost
  - Fewer rules (e.g., 27–64) underfit, increasing MSE by 30–60%
  - More rules (e.g., 216–343) offer <1% MSE improvement but 2–3× slower convergence

- **Justification for 125 Rules:**
  - Full coverage of input space (3 inputs × 5 MFs = 125 combinations)
  - Genetic Algorithm (GA) further prunes ineffective rules, retaining only the top 10 most impactful rules (see Table 5)

4.6.3 Generalizability across PV technologies

The fuzzy mechanism's stability across sample sizes and rule configurations confirms its adaptability to eventual existing of polycrystalline and thin-film panels, where parameter dynamics may differ. The GA-optimized rules ensure efficient performance even with limited data.

As a final conclusion, the proposed model achieves stable parameter identification with 200–250 training samples and 125 fuzzy rules, balancing accuracy and computational efficiency. This makes it viable for diverse PV technologies under real-world conditions.

5 Conclusion

This paper introduced a novel modeling approach for PV arrays, particularly those utilizing monocrystalline technologies, though applicable to other types as well. The proposed method relies on a PV model with adjustable and time-varying parameters, where the evolution of each parameter is supervised by a Fuzzy model. The rules were determined by the GA algorithm to minimize the MSE criterion between the actual and predicted currents. Unlike traditional fixed-parameter models, which often yield suboptimal modeling errors, the proposed PV model demonstrated superior performance during validation with real experimental measurements. The results confirmed that the proposed approach, combining Fuzzy with GA-based updates, provides a more accurate and reliable representation of the actual PV array's behavior. Moreover, this modeling approach offers a parametric framework that will be invaluable for future researchers in synthesizing MPPT controllers. It also facilitates comprehensive frequency analysis and robustness studies of the closed-loop system. In contrast, pure fuzzy models lack such parametric capabilities, limiting their utility for the closed-loop robustness analysis, frequency response evaluations, and similar studies.

Acknowledgement

All authors contributed equally to the research, analysis, writing, and editing of this article. Each author has approved the final version of the manuscript and agrees to its submission.

References

[1] H. Abid, I. Zaidi, A. Toumi, M. Chaabane, *T–S fuzzy algorithm for photovoltaic panel*, International Journal of Fuzzy Systems, **17**(2) (2015), 215-223. https://doi.org/10.1007/s40815-015-0025-4

[2] S. Aissani, S. Kahla, M. Bechouat, T. Amieur, M. Sedraoui, *A voltage PID controller synthesis based on a new small-signal linear model to enhance the performance of the standard P & O algorithm employed in photovoltaic panels*, Arabian Journal for Science and Engineering, (2023), 1-16. https://doi.org/10.1007/s13369-022-07494-x

[3] D. F. Alam, D. A. Yousri, M. B. Eteiba, *Flower pollination algorithm based solar PV parameter estimation*, Energy Conversion and Management, **101** (2015), 410-422. https://doi.org/10.1016/j.enconman.2015.05.074

[4] S. Alsadi, T. Khatib, *Photovoltaic power systems optimization research status: A review of criteria, constrains, models, techniques, and software tools*, Applied Sciences, **8**(10) (2018), 1761. https://doi.org/10.3390/app8101761

[5] A. Al-Subhi, M. I. Mosaad, T. A. Farrag, *PV parameters estimation using optimized deep neural networks*, Sustainable Computing: Informatics and Systems, **41** (2024), 100960. https://doi.org/10.1016/j.suscom.2024.100960

[6] A. Askarzadeh, L. dos Santos Coelho, *Determination of photovoltaic modules parameters at different operating conditions using a novel bird mating optimizer approach*, Energy Conversion and Management, **89** (2015), 608-614. https://doi.org/10.1016/j.enconman.2014.10.025

[7] R. Ayaz, *Self-tuning parameters of the proposed fuzzy immune integral controller to improve the performance of the standard P&O-MPPT strategy*, IEEE Access, (2024). https://doi.org/10.1109/ACCESS.2024.3519495

[8] R. Ayaz, I. Nakir, M. Tanrioven, *An improved MATLAB-Simulink model of PV module considering ambient conditions*, International Journal of Photoenergy, **2014** (2014). https://doi.org/10.1155/2014/315893

[9] M. Bechouat, M. Sedraoui, S. Aissani, *Improved INC-MPPT strategy based on new small-signal design model for solar system using frequency data extracted through graphical interface of plecs® software*, Arabian Journal for Science and Engineering, (2024), 1-14. https://doi.org/10.1007/s13369-023-08661-4

[10] M. Bechouat, A. Younsi, M. Sedraoui, Y. Soufi, L. Yousfi, I. Tabet, K. Touafek, *Parameters identification of a photovoltaic module in a thermal system using meta-heuristic optimization methods*, International Journal of Energy and Environmental Engineering, **8**(4) (2017), 331-341. https://doi.org/10.1007/s40095-017-0252-6

[11] Q. Bo, W. Cheng, M. Khishe, M. Mohammadi, A. H. Mohammed, *Solar photovoltaic model parameter identification using robust niching chimp optimization*, Solar Energy, **239** (2022), 179-197. https://doi.org/10.1016/j.solener.2022.04.056

[12] E. Çelik, M. Karayel, D. Maden, M. Abdel-Salam, N. Öztürk, O. Kaplan, M. Baljon, *Reconfigured single-and double-diode models for improved modelling of solar cells/modules*, Scientific Reports, **15**(1) (2025), 2101. https://doi.org/10.1038/s41598-025-86063-2

[13] A. A. Z. Diab, H. M. Sultan, T. D. Do, O. M. Kamel, M. A. Mossa, *Coyote optimization algorithm for parameters estimation of various models of solar cells and PV modules*, IEEE Access, **8** (2020), 111102-111140.

[14] K. M. El-Naggar, M. R. AlRashidi, M. F. AlHajri, A. K. Al-Othman, *Simulated annealing algorithm for photovoltaic parameters identification*, Solar Energy, **86**(1) (2012), 266-274. https://doi.org/10.1016/j.solener.2011.09.032

[15] A. Gontean, et al., *A novel high accuracy PV cell model including self-heating and parameter variation*, Energies, **11**(1) (2017), 36. https://doi.org/10.3390/en11010036

[16] K. Górecki, E. Krac, *Measurements of thermal parameters of solar modules*, Journal of Physics: Conference Series, **709**(1) (2016). https://doi.org/10.1088/1742-6596/709/1/012007

[17] A. Hadjaissa, K. Ameur, M. S. Ait Cheikh, N. Essounbouli, *A PSO-based optimization of a fuzzy-based MPPT controller for a photovoltaic pumping system used for irrigation of greenhouses*, Iranian Journal of Fuzzy Systems, **13**(3) (2016), 1-18. https://doi.org/10.22111/ijfs.2016.2426

[18] C. H. Hussaian Basha, C. Rani, *Performance analysis of MPPT techniques for dynamic irradiation condition of solar PV*, International Journal of Fuzzy Systems, **22**(8) (2020), 2577-2598. https://doi.org/10.1007/s40815-020-00974-y

[19] M. S. Ismail, M. Moghavvemi, T. M. I. Mahlia, *Characterization of PV panel and global optimization of its model parameters using genetic algorithm*, Energy Conversion and Management, **73** (2013), 10-25. https://doi.org/10.1016/j.enconman.2013.03.033

[20] D. Izci, S. Ekinci, A. G. Hussien, *Efficient parameter extraction of photovoltaic models with a novel enhanced prairie dog optimization algorithm*, Scientific Reports, **14**(1) (2024), 7945. https://doi.org/10.1038/s41598-024-58503-y

[21] S. Kahla, et al., *Enhanced the modeling accuracy by the design of new photovoltaic models including the proposed nonlinear thermal resistors*, International Journal of Modelling and Simulation, **43**(4) (2023), 507-522. https://doi.org/10.1080/02286203.2022.2094646

[22] A. Kazemian, et al., *Optimization of a novel photovoltaic thermal module in series with a solar collector using Taguchi based grey relational analysis*, Solar Energy, **215** (2021), 492-507. https://doi.org/10.1016/j.solener.2021.01.006

[23] K. Lappalainen, M. Piliougine, S. Valkealahti, G. Spagnuolo, *Photovoltaic module series resistance identification at its maximum power production*, Mathematics and Computers in Simulation, **224** (2024), 50-62. https://doi.org/10.1016/j.matcom.2023.05.021

[24] M. Premkumar, P. Jangir, C. Ramakrishnan, G. Nalinipriya, H. H. Alhelou, B. S. Kumar, *Identification of solar photovoltaic model parameters using an improved gradient-based optimization algorithm with chaotic drifts*, IEEE Access, **9** (2021), 62347-62379. https://doi.org/10.1109/ACCESS.2021.3073821

[25] M. Sedraoui, M. Bechouat, R. Ayaz, Y. Z. Alharthi, A. Borni, L. Zaghba, S. S. Ghoneim, *Development of a fixed-order controller for a robust P&O-MPPT strategy to control poly-crystalline solar PV energy systems*, Scientific Reports, **15**(1) (2025), 2923. https://doi.org/10.1038/s41598-025-86477-y

[26] Z. Tang, K. Wang, Y. Yao, M. Zhu, L. Zhuang, H. Chen, S. Gao, *Parameter adaptive manta ray foraging optimization for global continuous optimization problems and parameter estimation of solar photovoltaic models*, International Journal of Computational Intelligence Systems, **18**(1) (2025), 29. https://doi.org/10.1007/s44196-025-00753-3

[27] J. Wang, B. Yang, D. Li, C. Zeng, Y. Chen, Z. Guo, T. Yu, *Photovoltaic cell parameter estimation based on improved equilibrium optimizer algorithm*, Energy Conversion and Management, **236** (2021), 114051. https://doi.org/10.1016/j.enconman.2021.114051

[28] X. Wen, et al., *Performance analysis of a concentrated system with series photovoltaic/thermal module and solar thermal collector integrated with PCM and TEG*, Energy, **249** (2022), 123777. https://doi.org/10.1016/j.energy.2022.123777

[29] B. Yang, J. Wang, X. Zhang, T. Yu, W. Yao, H. Shu, L. Sun, *Comprehensive overview of meta-heuristic algorithm applications on PV cell parameter identification*, Energy Conversion and Management, **208** (2020), 112595. https://doi.org/10.1016/j.enconman.2020.112595

[30] M. E. F. Zagrouba, et al., *Identification of PV solar cells and modules parameters using the genetic algorithms: Application to maximum power extraction*, Solar Energy, **84**(5) (2010), 860-866. https://doi.org/10.1016/j.solener.2010.02.012